JOURNAL OF AIRCRAFT
Vol. 34, No. 2, March–April 1997

Automated Design Optimization for the P2 and P8 Hypersonic Inlets

Vijay Shukla,* Andrew Gelsey,† Mark Schwabacher,‡ Donald Smith,§ and Doyle D. Knight¶
Rutgers University, New Brunswick, New Jersey 08903

An automated design methodology incorporating industry-standard Navier–Stokes codes and a gradient-based optimizer has been developed. This system is used to redesign the well-known NASA P2 and P8 hypersonic inlets. First, the Navier–Stokes simulations of the original P2 and P8 inlet designs are validated using numerical convergence studies and comparison with wind-tunnel experimental data for the original inlets published by NASA in the early 1970s. Second, the P2 and P8 inlets are redesigned with the objective of canceling the cowl shock (and, in the case of the P8 inlet, the additional cowl-generated compression) at the centerbody by appropriate contouring of the centerbody boundary. The original inlets were intended to achieve these same objectives, but detailed experimental measurements indicated that a substantial reflected shock system was present. The choice of the objective function, which is used to drive the optimization, has a significant impact on the final design. Several different formulations for the objective function have been employed, and improvements of 60–90% in the objective function have been achieved. This automated design system represents one of the first successful combinations of numerical optimization methods with Reynolds-averaged Navier–Stokes fluid dynamics simulation for high-speed inlets, and demonstrates a new area in which high-performance computing may have considerable impact on problems of military and industrial significance.

Nomenclature

N_{BL} = number of points in incoming centerbody boundary layer
$N_{\mathrm{cent_{BL}}}$ = number of points in centerbody boundary layer at throat
$N_{\mathrm{cowl_{BL}}}$ = number of points in cowl boundary layer at throat
$\Delta y|_{\max}$ = height of grid cell with greatest y extent
Δy_2^+ = nondimensional estimate of resolution of viscous sublayer on centerbody = $\Delta y_2 u_* / \nu_w$, where $u_* = \sqrt{\tau_w/\rho_w}$ and τ_w = local shear at the wall = $\mu_w(\partial u/\partial n)$
δ_0 = thickness of incoming centerbody boundary layer, $\approx$1.1 cm at inlet entrance, x = 81.28 cm
σ_p, $\sigma_{\bar{p}}$, σ_{sh} = objective functions
σ_{p_t}, r_p, r_{p_t} = measures used in optimization

I. Introduction

RECENTLY there has been work on integrating design and computational fluid dynamics (CFD). Compared to wind-tunnel testing of designs, this process is lower in cost and can be completed in a relatively short period of time. For example, experimentally validated Navier–Stokes codes have been developed and used for turbomachinery design.[1] Typically, these codes are used by expert designers, who guide the selection of designs and shape modifications. Improvements are achieved by a manual, labor-intensive process. The complex flows in aerodynamic applications make it unlikely to attain optimum designs manually. Automatic design optimization techniques are thus essential to exploit the potential gains of using CFD in the design process.

Recently there has been work to automate the design process. This involves a description of the shape by a set of parameters and an objective function that describes the desired design goal. Aerodynamic shape optimization of inlets has been performed to minimize the peak inlet Mach number.[2] Nonlinear optimization has also been used in inlet design by coupling optimization with an inviscid flow solver to minimize total pressure loss.[3] Optimum shape design for minimization of drag for high-speed civil transport has been investigated using a simulated annealing algorithm.[4] Genetic algorithm-based optimization has been used for drag minimization over aerofoils.[5] A simplified scramjet-afterbody configuration has been optimized for axial thrust, using sensitivity analysis and analytical expressions for derivatives used in the optimization.[6] Optimization techniques based on control theory, which use adjoint equations for gradient calculation, are used for aerofoil and wing design.[7,8]

We have developed a prototype software system that combines Navier–Stokes simulations and numerical optimization methods. This system has been tested by redesigning the P2 and P8 inlets. The P2 and P8 inlets[9] were designed in the 1970s for a proposed hypersonic cruise vehicle for Mach 10 to 12. Models were built at approximately one-third scale and tested in the NASA Ames Research Center's 3.5-ft hypersonic wind tunnel. There was a forebody wedge of 6.5 deg, intended to match a design Mach number of 6 at the inlet entrance under the test conditions of a freestream Mach number of 7.4 (see Fig. 1). The freestream conditions at the entrance to the inlet were M = 5.8, p_{t_0} = 2.69 × 10^6 Pa, T_{t_0} = 770 K, and the incoming centerbody boundary layer was turbulent and had a thickness of δ_0 = 1.1 cm. The cowl was designed with a leading-edge diameter of 0.114 cm and both centerbody and cowl were cooled to maintain a temperature of 302 K. The P2 inlet cowl boundary layer was laminar. In the case of the P8 inlet, the cowl boundary layer transitioned from laminar to turbulent halfway between the cowl leading edge and the throat station. In the P2 inlet, a pressure rise by a factor of 2 (thus the name

Received Dec. 30, 1995; revision received Oct. 22, 1996; accepted for publication Dec. 30, 1996.

*Postdoctoral Research Associate, Department of Mechanical and Aerospace Engineering. Member AIAA.
†Assistant Professor, Computer Science Department. Member AIAA.
‡Graduate Student, Computer Science Department.
§Assistant Professor, Computer Science Department.
¶Professor, Department of Mechanical and Aerospace Engineering. Associate Fellow AIAA.

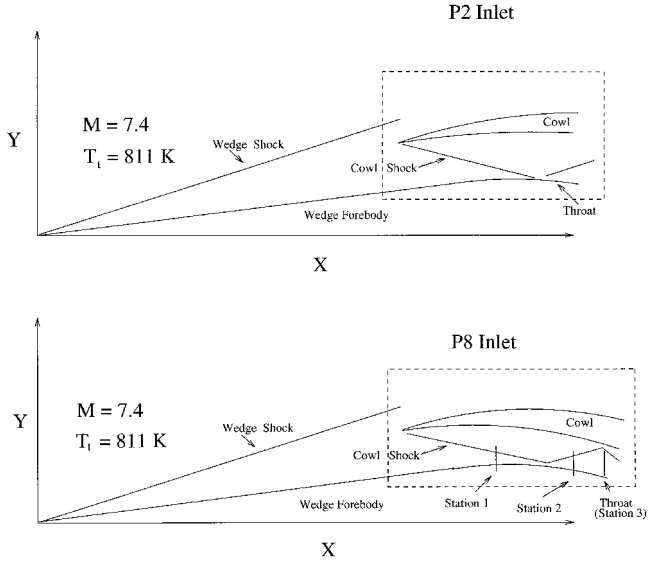

Fig. 1 Schematic diagram showing the P2 and P8 inlets. The computational domain is shown by dotted lines.

P2) was obtained by the shock generated at the cowl leading edge. In the case of the P8 inlet, the pressure rose by a factor of 2 across the cowl shock, and an additional factor of 4 of compression was obtained by a compression wave system generated by the curvature of the cowl. Extensive experimental data were gathered by Gnos et al.[9] Since then, several researchers[10,11] have performed two-dimensional Navier–Stokes simulations of these inlets, the earliest being Knight.[12]

The original internal contours were designed with the objective of providing high total pressure recovery and approximately uniform static pressure at the throat. To meet this objective, it was deemed essential to cancel the incident shock (and additional compression system in the case of the P8 inlet) through surface turning at the point of impingement of the shock on the centerbody.[9] The necessary surface turning was computed using the method of characteristics in conjunction with a boundary-layer model. The experimental results, however, showed that the cowl shock was not canceled by the centerbody contour for either inlet.

We select as our objective the same goal as was used in the original NASA study, namely, to cancel the incident cowl shock (and in the case of the P8 inlet, additional cowl compression) through redesign of the centerbody surface geometry, while retaining the same approximate overall static pressure rise. The cowl surface is unchanged, thereby yielding the same incident wave system as the original inlets. The achievement of our objective would imply an approximately uniform static pressure at the inlet throat, which is a condition generally considered desirable at the combustor entrance.[9]

II. Validation of CFD Codes

It is essential to confirm that the flows in the P2 and P8 inlets, which are characterized by high Mach number, high gradient of flow variables near shocks, and shock boundary-layer interactions, are accurately predicted by the CFD codes. This is a precondition for any redesign using CFD codes. The GASPv2.2 (General Aerodynamic Simulation Program from Aerosoft Inc.[13]) and NPARCv2.1[14,15] codes are employed for the Navier–Stokes simulations. As indicated later, they accurately predict the flows in the P2 and P8 inlets.

The NPARC code, which is employed for P2 optimizations, uses the Beam–Warming approximate factorization algorithm. The GASP code, which is employed for P8 optimizations, uses Roe's method for the inviscid fluxes and central differencing for the viscous stresses and heat transfer. For both P2 and P8 calculations, turbulence is incorporated using the k-ε model with the Chien low Reynolds number correction.[16] We use the Chien k-ε model[16] in the EDDYBL turbulent boundary-layer code of Wilcox[17] to generate the inflow profile immediately upstream of the inlet that matched the experimental conditions. This profile is used as a fixed upstream boundary condition for the CFD codes and is propagated throughout the domain to give an initial flowfield for the calculations.

Prior to optimization, we performed a grid refinement study for the original P2 and P8 inlets. Tables 1 and 2 show properties of each grid. In constructing the grids, the shape of the inlet is determined using spline interpolation through the (x, y) points specified in Table 1 of Gnos et al.[9] However, the leading edge of the cowl is extended 2.79 cm upstream to correctly position the shock wave generated by the cowl. This adjustment, identical to the technique employed by Knight,[12] is required since the details of the blunt-body shock in the immediate vicinity of the cowl leading edge are not resolved. Our grids use equal spacing in the x direction and exponential spacing in the y direction (near both the cowl and centerbody) with an upper limit on cell growth. The experimental data[9] indicate an incoming centerbody boundary-layer thickness δ_0 of 1.1 cm, and Tables 1 and 2 show that the number of points our grids have in this centerbody boundary layer compares favorably

Table 1 Properties of grids used in convergence study in P2 simulation

Property	Grid 1	Grid 2	Grid 3
x points	121	241	481
y points	83	165	329
N_{BL}	46	92	183
$N_{cowl_{BL}}$	8	15	26
$N_{cent_{BL}}$	46	95	190
y expansion ratio	1.15	1.0724	1.0364
$\Delta x/\delta_0$	0.380	0.190	0.0939
$\Delta y\|_{max}/\delta_0$	0.375	0.188	0.0950
$\Delta y^+_2\|_{average}$	0.153	0.0681	0.0324
σ_p	0.06986	0.07282	0.07614
r_p	2.0053	1.9514	1.9413
σ_{p_t}	0.3942	0.3775	0.3832
r_{p_t}	0.4957	0.5163	0.5187
CPU seconds/iteration[a]	0.97	4.8	33
Iterations needed	6000	25,000	25,000
Total compute time[b]	1.6 hours	1.4 days	9.5 days

[a]On Hewlett–Packard 735/125 workstation, using single precision.
[b]On Hewlett–Packard 735/125 workstation.

Table 2 Properties of grids used in convergence study in P8 simulation

Property	Grid 1	Grid 2	Grid 3
x points	138	138	275
y points	101	151	301
N_{BL}	40	57	114
$N_{cowl_{BL}}$	30	52	106
$N_{cent_{BL}}$	40	62	122
y expansion ratio	1.20	1.15	1.0724
$\Delta x/\delta_0$	0.344	0.344	0.172
$\Delta y\|_{max}/\delta_0$	0.24	0.225	0.1125
$\Delta y^+_2\|_{average}$ centerbody	0.44	0.147	0.0737
$\Delta y^+_2\|_{average}$ cowl	1.1	0.36	0.18
σ_p	0.143	0.147	0.137
$\sigma_{\bar{p}}$	0.176	0.189	0.199
σ_{sh}	0.269	0.267	0.286
r_p	8.482	8.469	8.365
σ_{p_t}	0.461	0.464	0.444
r_{p_t}	0.451	0.449	0.461
CPU seconds/iteration[a]	4.5	6.5	30.0
Iterations needed	3700	4700	20000
Total compute time[b]	4.6 hours	8.5 hours	166 hours

[a]On DEC-Alpha 2100 workstation, using single precision.
[b]On DEC-Alpha 2100 workstation.

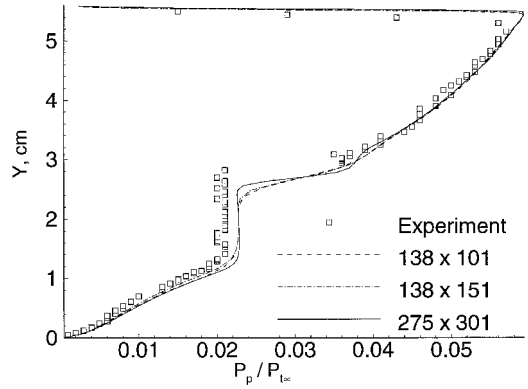

Fig. 2 Pitot pressure at station 1, x = 1.0414 m, for original P8 inlet. (Y axis shows centimeters measured vertically from centerbody. Experimental data is from Fig. 44a of Ref. 9.)

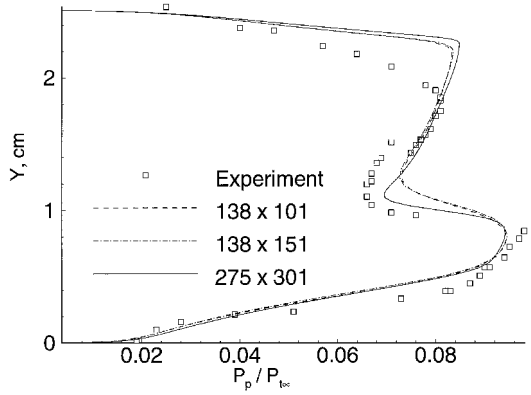

Fig. 3 Pitot pressure at station 2, x = 1.1938 m, for original P8 inlet. (Y axis shows centimeters measured vertically from centerbody. Experimental data is from Fig. 44i of Ref. 9.)

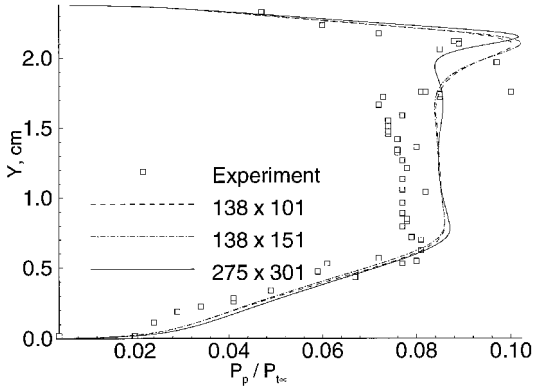

Fig. 4 Pitot pressure at (throat) station 3, x = 1.2573 m, for original P8 inlet. (Y axis shows centimeters measured vertically from centerbody. Experimental data is from Fig. 44m of Ref. 9.)

with the 30 points suggested by the traditional rule of thumb. These tables provide values of $\Delta y_2^+|_{\text{average}}$ computed from our converged NPARC/GASP solutions, indicating an adequate resolution of the viscous sublayer on the cowl and centerbody. The values of objective functions measures of merit defined in Sec. III.C are also listed (Tables 1 and 2). On the basis of the grid refinement studies, we conclude that the numerical uncertainty in the objective functions is ±10%. During computations of the inlets the L2 residual drops by four orders of magnitude.[18,19]

Our flow simulations for the P2 and P8 inlets are in good agreement with experiments of Gnos et al.,[9] thereby justifying the use of GASP/NPARC in optimization. The results of this simulation are of similar accuracy to those obtained by other authors.[10–12] In the interests of brevity, only comparisons of experimental and computed pitot pressure profiles for the P8 inlet at stations 1, 2, and 3 of Fig. 1 are presented. Further details for P2 and P8 inlets are available in Refs. 18 and 19, respectively. Figure 2 shows both the experimental and computed pitot pressure for the P8 inlet at x = 1.0414 m, where the freestream pressure upstream of the wedge P_∞ = 701.4 Pa is used to nondimensionalize pressure and $p_{t_\infty} = 4.14 \times 10^6$ Pa is used to nondimensionalize the pitot pressure. The cowl shock is apparent in both the experiment and computations as a jump in pitot pressure at Y = 2.8 cm. The centerbody boundary layer and shock location agree well with the experiment. Omission of the cowl entropy layer causes a slight discrepancy near the cowl. Figure 3 shows the experimental and computed pitot pressure for the P8 inlet at X = 1.1938 m, which is downstream of the boundary-layer interaction, and Fig. 4 displays the results at the throat. The agreement between computation and experiment is good, with the discrepancies confined to the vicinity of the cowl surface because of the omission of the cowl entropy layer. Figures 2–4 also show that the results indicate grid convergence, except for the expected refinement of the shock. Similar agreement is found during simulation of the P2 inlet.[19]

III. Redesign of the P2 and P8 Inlets

The design objective is chosen to be the same as the original NASA study, namely, to cancel the cowl shock (and cowl-generated compression in the P8 inlet) at the centerbody. Our automated design methodology changes the centerbody shape to achieve this goal while maintaining the required pressure rise. Our redesign of the inlets consists of a loop of three steps. Firstly, a parameterized space of candidate redesigns is defined. Next, the space of candidate redesigns is searched automatically using a numerical optimization method. And finally, the objective function (measure of merit) is reconsidered to achieve the objective of shock cancellation. These steps are described in detail in the following text.

A. Parameterized Geometry Model

All inlets in our parameterized space of candidate redesigns use the same cowl contour as the original NASA inlets. This enables our new inlet designs to have approximately the same compression ratios as the original P2 and P8 inlets. We replace the original centerbody contour with a parameterized contour consisting of three sections shown in Fig. 5. The left section is a straight line rising at angle θ, which terminates at point (x_l, y_l). The right section is a straight line turned through angle Δθ relative to the left line, starting at a point offset by $(\Delta x, \Delta y)$ from the end of the left section. The middle section is a smooth curve whose shape is uniquely determined by the requirement that it connect the left and right sections, have an angle of θ_1 at (x_l, y_l), and match the slope at $(x_l + \Delta x, y_l + \Delta y)$. This smooth curve is parametrically generated as follows:

$$\begin{bmatrix} x \\ y \end{bmatrix} = \begin{bmatrix} x_c \cos p + x_s \sin p + x_0 \\ y_c \cos p + y_s \sin p + y_0 \end{bmatrix}, \qquad 0 \le p \le \frac{\pi}{2}$$

and the six coefficients are uniquely determined (except in the Δθ = 0 case) by the following requirements:

p	$x(p)$	$y(p)$	angle
0	x_l	y_l	θ_1
π/2	$x_l + \Delta x$	$y_l + \Delta y$	$\theta + \Delta\theta$

The centerbody contour for our redesigned inlets is mathematically defined to be the portion of this parameterized contour that lies between the upstream and downstream boundaries of our computational domain. This mathematical definition does not require that the portion of the parameterized contour within the computational domain include all three sections of the full parameterized curve shown in Fig. 5.

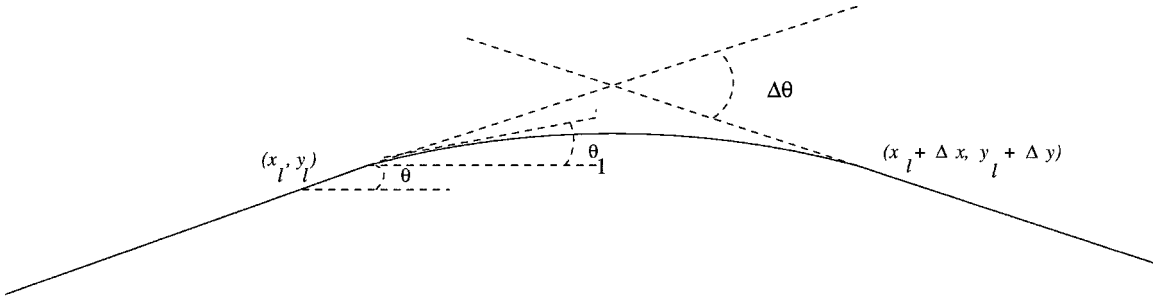

Fig. 5 Parameterized contour for redesign of P8 inlet centerbody.

B. Numerical Optimization

We use a set of *C* functions known as CFSQP, described in Ref. 20, to perform the optimization. CFSQP minimizes an objective function subject to general smooth constraints. The package uses the sequential quadratic programming (SQP) method to solve a nonlinear programming problem by solving a sequence of quadratic programming problems as follows: 1) fit a quadratic programming problem to the nonlinear programming problem, 2) solve the quadratic programming problem, 3) perform a search along the line defined by the current point and the minimum of the quadratic programming problem for a point that improves the objective function while satisfying all constraints, and 4) repeat.

Fitting a quadratic program to the objective function is done by computing the Hessian of the objective function with respect to design vector, and the gradient of each constraint function with respect to the design vector. Since computing the Hessian is expensive, an approximation of the inverse of the Hessian, known as the quasi-inverse Hessian, is used. The quasi-inverse Hessian is updated on each iteration using the gradient of the objective function. In CFSQP, this update is done using the Broyden-Fletcher-Goldfarb-Shanno update formula. SQP is thus a quasi-Newton method.

Solving a quadratic programming problem is a much easier task than solving an arbitrary nonlinear programming problem. CFSQP uses the package QLD, an implementation of Powell's method of solving quadratic programming problems, to solve the quadratic programming problem at each iteration.

CFSQP terminates when one of two conditions is met. The first condition is that the solution of the quadratic programming problem is within a certain tolerance of the current point. This means that, according to the quadratic approximation, the current point is approximately the minimum. The second condition is that the improvement in the objective function during the line minimization is less than a certain tolerance. More details on implementation may be found in Refs. 18 and 19.

C. Quantitative Measures of Flow

The measures used during optimization can be divided into two main categories. The first category, the objective function, is used to drive the optimizer and the second is used to restrict the domain of the objective function to include only physically realizable designs. The optimizer minimizes a measure from the first category subject to the condition that constraints in the second category are not violated. The objective functions investigated are described next:

1) A local measure, static pressure distortion at the throat, defined by

$$\sigma_p \equiv \frac{1}{\bar{p}}\left[\frac{1}{H}\int_0^H (p - \bar{p})^2\, dy'\right]^{1/2}$$

where $\bar{p}$ is the mean static pressure at the throat

$$\bar{p} \equiv \frac{1}{H}\int_0^H p\, dy'$$

where H is the height of the throat and y' is measured (vertically) from the lower surface.

2) A volumetric measure, average static pressure distortion $\sigma_{\bar{p}}$, which is a normalized standard deviation of static pressure $p(x, y)$, is defined as follows:

For all n cells in the vicinity of the reflected shock (1.19868 m $< x <$ 1.26322 m)

$$\bar{p} = \left[\frac{\sum p(x, y)}{n}\right] \qquad \sigma_{\bar{p}} = \frac{1}{\bar{p}}\left\{\frac{\sum [p(x, y) - \bar{p}]^2}{n - 1}\right\}^{1/2}$$

This region contains a portion of the reflected shock in the original P8 inlet, while omitting all of the cowl-generated compression waves. The rationale for this is that reduction in this measure would reduce the strength of the reflected shock at the centerbody.

3) A physics-based measure intended to directly measure shock strength is defined as follows:

For all n_y cells at a given x location

$$\bar{p}_x = \frac{\sum_{n_y} p(x, y)}{n_y} \qquad \sigma_{\text{sh}} = \frac{1}{n_x}\sum_{n_x}\left(\frac{\Delta p}{\bar{p}_x}\right)$$

where Δp is the static pressure jump across the shock, $p(x, y)$ is the static pressure distribution, and n_x cells are used in the x direction.

The constraints employed include the following:

1) Mean static pressure recovery, defined by

$$r_p \equiv \frac{1}{Hp_\infty}\int_0^H p\, dy'$$

where p_∞ is the static pressure immediately upstream of the inlet entrance.

2) Total pressure distortion at the throat, defined by

$$\sigma_{p_t} \equiv \frac{1}{\bar{p}_t}\left[\frac{1}{H}\int_0^H (p_t - \bar{p}_t)^2\, dy'\right]^{1/2}$$

where $\bar{p}_t$ is the mean total pressure at the throat:

$$\bar{p}_t \equiv \frac{1}{H}\int_0^H p_t\, dy'$$

3) Mean relative total pressure at the throat, defined by

$$r_{p_t} \equiv \frac{1}{Hp_{t_\infty}}\int_0^H p_t\, dy'$$

where p_{t_∞} is the upstream freestream total pressure measured in the freestream flow at the entrance to the inlet.

Tables 1 and 2 show the various measures for the original P2 and P8 geometries; all improved designs will be compared

with these numbers. To reduce CPU time, Grid 1 in Tables 1 and 2 (P2: 121 × 83 and P8: 138× 101) are used during the optimization. It can also be seen from Table 1 that changing from single to double precision did not change the measures significantly. Taken together, Tables 1 and 2 show that the numerical uncertainty in measures is probably less than 10% for the grids used in optimization (since variations of about 6–7% occur when grids are doubled).

D. Optimization Procedure

We configure CFSQP to minimize the objective function by simultaneously varying, in the most general case, the five parameters x_l, θ_1, $\Delta\theta$, Δx, and Δy in Fig. 5. We therefore have a five-dimensional space of candidate inlet designs through which to search and find an optimal design. All CFD simulations during the numerical optimization are performed using Grid 1 in Tables 1 and 2. This gave acceptable accuracy and CPU time requirements during optimization. The value of θ is fixed as 0.11738 rad, and y_l is computed by

$$y_l = x_l \tan\theta - 0.001122 \text{ m}$$

These values make the ramp (left section) of the redesigned centerbody coincide as closely as possible with the ramp of the original inlets.

Because of the large computational time required, not all optimizations varied all five parameters. For the P2 optimization $\theta_1 = 0.11738$. Two parameters are kept fixed in the initial P8 optimizations. The parameter θ_1 is fixed at 0.11738 rad and the parameter $\Delta\theta$ is fixed at 0.291 rad, so that the centerbody and cowl are parallel for $x > x_l + \Delta x$. In the original designs also, the centerbody and cowl contours downstream of the location where design pressures were obtained were designed to provide uniform flow and maintain the pressure ratio by staying approximately parallel.

To find an optimal redesign of the inlets, we automatically search our space of candidate designs using CFSQP. Several measures are used by CFSQP: some are used as constraints, some are monitored, and one is used as the function that is minimized. Loose constraints on the mean static pressure recovery r_p (P2: $1.9 \le r_p \le 2.1$ and P8: $7.5 \le r_p \le 8.5$) are used so that an appropriate inlet static pressure rise is obtained. The measures σ_{P_t} and r_{P_t} are allowed to vary freely, but monitored to ensure that improvements in static pressure distortion did not require significant sacrifices in quality of the other measures of merit.

In addition to the design constraints, we use one model constraint.[21] This constraint specifies that the two line segments in Fig. 5, when extended into lines, cross at a horizontal location between x_l and $x_l + \Delta x$. We handle this model constraint in two ways. In some early optimizations, we use rule-based gradients.[22] The rules specify what to do when a point generated by CFSQP violates the model constraint. For example, it can revert from the central-difference formula to the forward-difference formula, or it can use a different step size to compute the partial derivative. In later optimizations, we explicitly pass the model constraint to CFSQP as two additional nonlinear inequality constraints.

IV. Results

In the optimal design of the P2 inlet, we minimize σ_p at the throat while letting x_l, Δx, Δy, and $\Delta\theta$ be determined by the optimizer. This virtually eliminates the reflected shock (see Fig. 6) and reduces σ_p by 80.1% (see Table 3) using 60 Navier–Stokes simulations, which corresponds to five days on a Hewlett–Packard 735/125 workstation. The reduced static pressure distortion at the throat can also be observed in Fig. 7. As indicated in Table 4, the optimal Δx is 0.4705 m, which is more than six times the distance from x_l to the throat (x = 1.1938 m). Since Δy is small, the centerbody is therefore effectively a wedge forebody joined to a straight line segment. At the optimum this line segment is also approximately horizontal. It has been found that using only x_l as a free parameter in a simpler formulation for the centerbody geometry ($\Delta x = 0$, $\Delta y = 0$, and $\Delta\theta$ are chosen so that the centerbody is approxi-

Table 3 Measures of merit for original P2 inlet and best redesigned P2 inlet[a]

Measure	Original	Optimal	Change, %
σ_P	0.0699	0.0134	−80.1
r_P	2.0053	1.9238	−4.1
σ_{P_t}	0.3942	0.4014	1.8
r_{P_t}	0.4957	0.4926	0.6

[a]Both computed using grid 1.

Table 4 Design parameters for optimal redesigned P2 and P8 inlets, for different measures of merit

Geometry parameter	P2 inlet	P8 inlet		
	σ_P	σ_P	$\sigma_{\bar{P}}$	σ_{sh}
x_l, m	1.1189	1.1092	1.1448	1.13097
Δx, m	0.4705	0.1150	0.06973	0.1500
Δy, m	−0.0013	−0.0038	−0.00689	−0.01687
θ_1, rad	0.11738	0.11738	−0.08998	0.11738
$\Delta\theta$, rad	0.1249	0.291	0.298	0.291

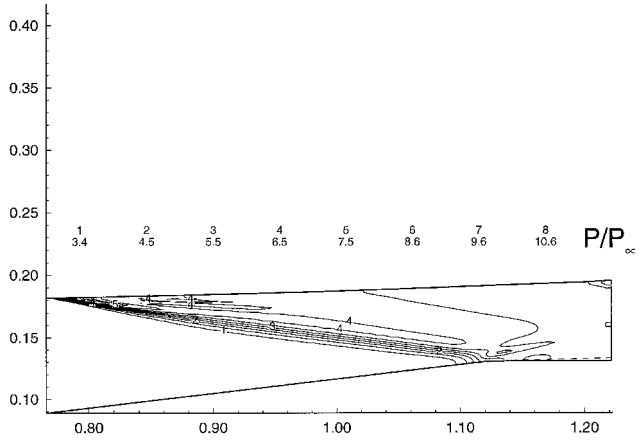

Fig. 6 Pressure contours computed by NPARC for optimal redesigned P2 inlet using the σ_p objective function. Dimensions are in meters. The original centerbody contour is shown by a dotted line.

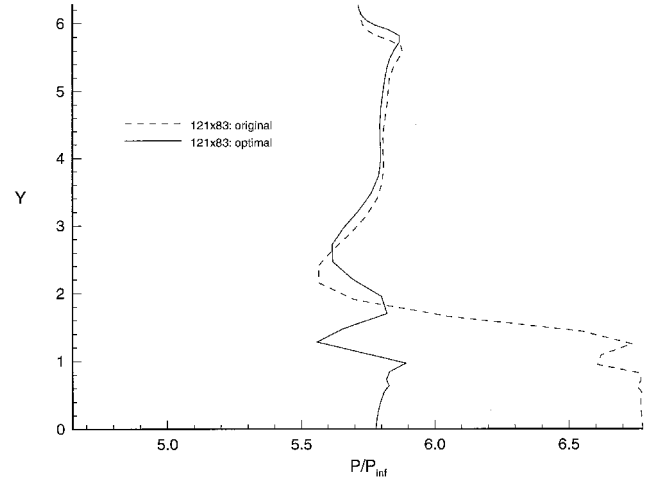

Fig. 7 Static pressure profile at the throat (station at x = 1.1938 m) for original and optimized P2 inlets. Y axis shows centimeters measured vertically from centerbody.

Table 5 Measures of merit for starting point P8 inlet and best redesigned P8 inlets using σ_P, $\sigma_{\bar{P}}$ and σ_{sh} (all computed with grid 1)[a]

Measure name	Original inlet	Objective σ_P		Objective $\sigma_{\bar{P}}$		Objective σ_{sh}	
		Optimal	Change, %	Optimal	Change, %	Optimal	Change, %
σ_P	0.1434	**0.0304**	**−78.8**	0.0159	−88.9	0.148	3.2
$\sigma_{\bar{P}}$	0.1763	0.1226	−30.5	**0.0603**	**−65.7**	0.1496	−15.1
σ_{sh}	0.2688	0.198	−26.3	0.1102	−59.0	**0.027**	**−89.9**
r_P	8.481	7.85	−7.4	7.503	−11.5	7.541	−11.1
σ_{P_t}	0.4605	0.4786	3.9	0.4803	4.3	0.465	1.0
r_{P_t}	0.4505	0.4471	−0.8	0.4528	0.5	0.461	2.3

[a]The objective function used during optimization is in bold, other measures are shown for comparison purposes.

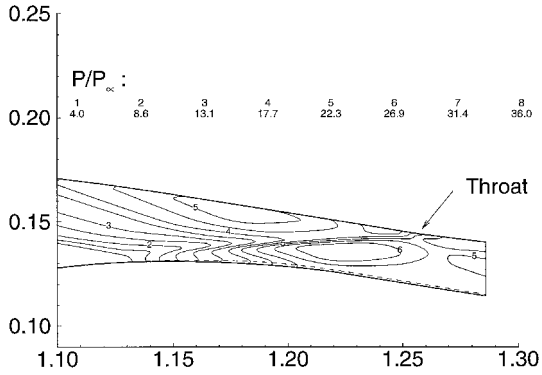

Fig. 8 Pressure P/P_∞ computed by GASP for optimal redesigned P8 inlet using the σ_P objective function. Dimensions are in meters. The original centerbody contour is shown by a dotted line.

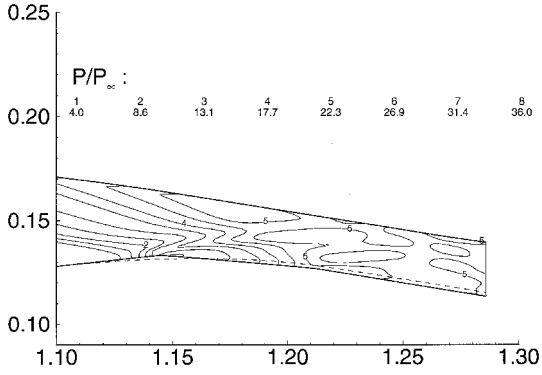

Fig. 9 Pressure P/P_∞ computed by GASP for optimal redesigned P8 inlet using the $\sigma_{\bar{P}}$ objective function. Dimensions are meters. The original centerbody contour is shown by a dotted line.

mately horizontal for $x > x_l$) can also effectively cancel the shock and reduce σ_P by ≈74%. This one-parameter optimization takes only 10 Navier–Stokes simulations compared to 60 for the four-parameter optimization, thus reducing the CPU time required to 0.8 days from 5.0 days on a Hewlett–Packard 735/125 workstation.

In our optimal design of the P8 inlet we first attempted to minimize the reflected shock using the static pressure distortion σ_P at the inlet throat as an objective function. This optimization varied the parameters x_l, Δx, and Δy. As seen in Fig. 8, this is not effective in canceling the shock, because the optimizer could position the shock in such a way as to minimize σ_P without canceling the shock (i.e., the reflected shock intersected the cowl at the throat). Indeed, for the original P8 geometry the reflected shock also intersected the cowl at approximately the throat location, thereby yielding an approximately uniform static pressure at the throat while nonetheless failing to cancel the incident cowl shock. This demonstrates that a proper selection of the objective function is important. Table 5 shows that σ_P was reduced by 78.8% in this measure without canceling the shock.

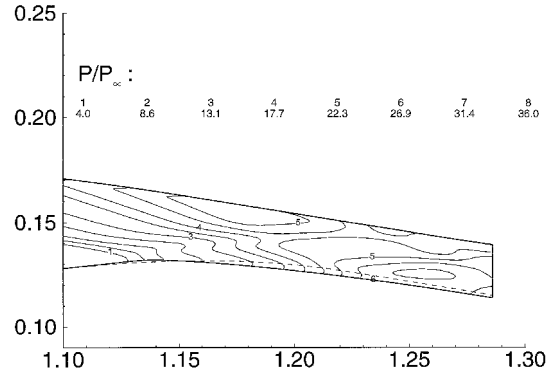

Fig. 10 Pressure P/P_∞ computed by GASP for optimal redesigned P8 inlet using σ_{sh} objective function. Dimensions are in meters. The original centerbody contour is shown by a dotted line.

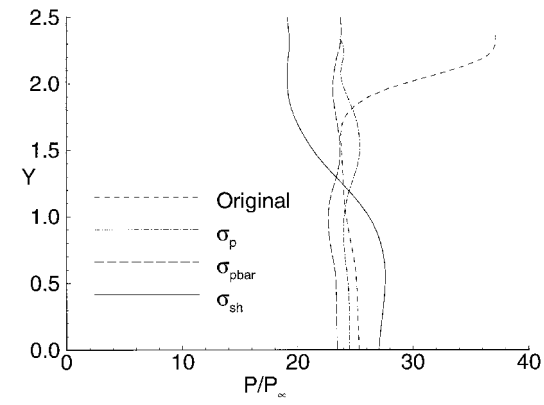

Fig. 11 Static pressure profile at the throat (station at x = 1.2573 m) for original and optimized P8 inlets. Y axis shows centimeters measured vertically from centerbody.

We next attempted the volumetric measure $\sigma_{\bar{P}}$ as the objective function. A reduction of 56% was obtained when x_l, Δx, and Δy were varied. To investigate the effect of a number of geometric parameters on optimization, we allowed the optimizer to also vary θ_1 and $\Delta\theta$. This five-parameter optimization resulted in an additional improvement of 9.7%. As seen in Fig. 9, the shock strength has been reduced, but shock cancellation does not occur. This measure has been reduced by a total of 65.7% (see Table 5, columns 5 and 6) for the five-parameter optimization. In this case, σ_P and σ_{sh} are reduced significantly.

Lastly, the shock strength measure σ_{sh} was used as an objective. This optimization varied x_l, Δx, and Δy. Figure 10 shows that minimization of this measure results in effective cancellation of the shock. This measure was reduced by 89.9% (see Table 4, columns 7 and 8). As seen in Figs. 10 and 11, the cancellation of the shock does not completely eliminate the static pressure distortion at the throat because the growth of the centerbody boundary layer causes additional compression waves.

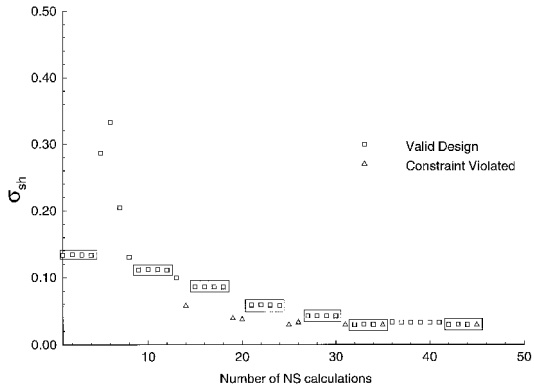

Fig. 12 Change in objective σ_{sh}, is shown in terms of the Navier–Stokes calculations. The parameters x_s, Δx, and Δy are varied in this optimization. The data points are square for a valid design, triangles for design with constraint violated, and the boxes show the groups of four Navier–Stokes calculations used in the gradient computation.

Table 4 shows the optimum values of the parameters of the geometric description of the centerbody for the P2 and P8 optimal inlets. In the P8 optimization, the σ_p measure does not reduce or cancel the shock, so the parameter values are far from those for $\sigma_{\bar{p}}$ and σ_{sh}, which are effective in reducing the shock strength. It can be observed that the pressure ratio r_p obtained by optimal designs is about 7.5. To obtain a pressure ratio closer to 8.0 and low static pressure distortion, the cowl geometry may need to be changed.

The sequence of designs for the three-parameter optimization using σ_{sh} as the objective function is shown in Fig. 12. At each iteration CFSQP computes a gradient, then computes a search direction from the gradient, and finally does a line search. Gradients are computed using forward differences; hence, each gradient requires four Navier–Stokes calculations for this three-parameter optimization. In Fig. 12, each gradient calculation is enclosed in a box. The line search varies the design parameters to move along a line in the specified direction. Within the line search, CFSQP first tries the full Newton step (stepping to the minimum of the quadratic programming problem), and if that does not improve the objective function while satisfying the constraint, it next tries smaller steps, and continues until it finds a point that improves the objective function and satisfies the constraint. In Fig. 12, the beginning of this optimization has a line search in which the σ_{sh} initially rises, causing this particular iteration to take eight Navier–Stokes evaluations. Once a reasonable approximation for the Hessian matrix is built up in the optimizer, σ_{sh} usually improves in the first step of each line search. Significant improvements are seen to take place within the first 30–40 Navier–Stokes evaluations.

In our redesign of the P8 inlet using σ_{sh} as an objective function, we used the geometry from the final point of a three-parameter $\sigma_{\bar{p}}$ optimization as a starting point. For all practical purposes this is a reasonable starting point. As seen in Fig. 12, convergence is achieved in approximately 25 Navier–Stokes computations. The optimization was allowed to proceed for 46 Navier–Stokes evaluations to ensure that an optimal geometry has been obtained. On the DEC Alpha 2100-4/275, this translates into 4.8 days for reaching the optimum and an additional four days to confirm that the optimum has been obtained.

V. Conclusions

An automated design methodology is applied to the redesign of the NASA hypersonic inlets. The methodology includes a Navier–Stokes code (NPARC or GASP), the gradient-based optimization method CFSQP, a multiparameter geometry model for the centerbody geometry, and constraints to ensure adequate static pressure rise. The chosen objective is the cancellation of the cowl shock (and distributed cowl-generated compression at the centerbody for the P8 inlet). This was also the intention of the original design.

The measure of static pressure distortion at the throat is successful in canceling the shock for the P2 inlet. This measure fails in the case of P8 because of the added complexity in the flow. Two of the mathematical criteria are successful in reducing the reflected wave strength for P8. The most successful method σ_{sh}, employing the direct computation of the average reflected shock strength, is reduced by 90%.

Acknowledgments

This research is part of the Hypercomputing and Design (HPCD) project based at Rutgers University. The HPCD project is supported by the Advanced Research Projects Agency of the Department of Defense through Contract ARPA-DABT 63-93-C-0064, which is monitored by Bob Lucas. We had very helpful discussions about inlet design with David Sobel and Marty Haas of the United Technologies Research Center, Gerald Paynter from Boeing Commercial Aircraft Co., and Richard Pelz and Madara Ogot from the Department of Mechanical and Aerospace Engineering at Rutgers University. We acknowledge the assistance of Sam Gao of the Department of Computer Science at Rutgers University in performing the P2 computations. Some computations have also been performed at the DOD Shared Resource Center: Naval Oceanographic Office at Stennis Space Center and at the DOD High Performance Computing Center USAE Waterways Experimental Station. Postprocessing was performed at the Rutgers University Supercomputer Remote Access Center. More information about our inlet design work, including our publications, is available via World Wide Web at http://www.cs.rutgers.edu/hpcd. This and other related papers are under the link for high-speed inlet design at the bottom of the HPCD homepage.

References

[1]Rhie, C. M., Zacharias, R. M., Hobbs, D. E., Sarathy, K. P., Biederman, B. P., Lejambre, C. R., and Spear, D. A., "Advanced Transonic Fan Design Procedure Based on a Navier-Stokes Method," *Journal of Turbomachinery*, Vol. 116, April 1994, pp. 291–297.

[2]Reddy, E. S., and Reddy, D. R., "Aerodynamic Shape Optimization of a Subsonic Inlet Using 3-D Euler Computation," AIAA Paper 95-2757, July 1995.

[3]Munipalli, R., Wadawadigi, G., Anderson, D. A., and Wilson, D. R., "Application of Optimization Techniques to Inlet Design," AIAA Paper 95-1824, June 1995.

[4]Aly, S., Marconi, F., Ogot, M., Pelz, R., and Siclari, M., "Stochastic Optimization Applied to CFD Shape Design," AIAA Paper 95-1647, July 1995.

[5]Yamamoto, K., and Inoue, O., "Application of Genetic Algorithm to Aerodynamic Shape Optimization," AIAA Paper 95-1650, June 1995.

[6]Baysal, O., and Eleshaky, M. E., "Aerodynamic Design Optimization Using Sensitivity Analysis and Computational Fluid Dynamics," *AIAA Journal*, Vol. 30, No. 3, 1992, pp. 718–725.

[7]Jameson, A., "Optimum Aerodynamic Design Using CFD and Control Theory," AIAA Paper 95-1729, July 1995.

[8]Kuruvila, G., Ta'asan, S., and Salas, M. D., "Aerofoil Optimization by the One-Shot Method," Special Course on Optimum Design Methods for Aerodynamics, Von Kármán Inst. for Fluid Dynamics, Rhode-Saint-Genese, Belgium, April 1994.

[9]Gnos, A. V., Watson, E. C., Seebaugh, W. R., Sanator, R. J., and DeCarlo, J. P., "Investigation of Flow Fields Within Large-Scale Hypersonic Inlet Models," TN D-7150, NASA, April 1973.

[10]Kapoor, K., Anderson, B. H., and Shaw, R. J., "Comparative Study of Turbulence Models in Predicting Hypersonic Inlet Flows," AIAA Paper 92-3098, July 1992.

[11]Ng, W. F., Ajmani, K., and Taylor, A. C., III, "Turbulence Modeling in a Hypersonic Inlet," *AIAA Journal*, Vol. 27, No. 10, 1989, pp. 1354–1360.

[12]Knight, D. D., "Numerical Simulation of Realistic High-Speed Inlets Using the Navier-Stokes Equations," *AIAA Journal*, Vol. 15, No. 11, 1977, pp. 1583–1589.

[13]McGrory, W. D., Slack, D. C., Applebaum, M. P., and Walters, R. W., ''GASP Version 2.2: The General Aerodynamic Simulation Program,'' Aerosoft Inc., Blacksburg, VA, 1993.

[14]Cooper, G. K., and Sirbaugh, J. R., ''PARC Code: Theory and Usage,'' Arnold Engineering Development Center, TR-89-15, Arnold AFB, TN, Dec. 1989.

[15]Sirbaugh, J. R., Smith, C. F., III, Towne, C. E., Cooper, G. K., James, R. R., III, and Power, G. D., *A Users Guide to NPARC Version 2.0*, NPARC Alliance, Arnold AFB, TN, Nov. 1994.

[16]Chien, K. Y., ''Predictions of Channel and Boundary-Layer Flows with a Low-Reynolds Number Turbulence Model,'' *AIAA Journal*, Vol. 20, No. 1, 1982, pp. 33–38.

[17]Wilcox, D. C., ''Turbulence Modeling for CFD,'' DCW Industries, Inc., La Cañada, CA, 1993.

[18]Shukla, V., Gelsey, A., Schwabacher, M., Smith, D., and Knight, D. D., ''Automated Redesign of the NASA P8 Hypersonic Inlet Using Numerical Optimization,'' AIAA Paper 96-2549, July 1996.

[19]Gelsey, A., Knight, D. D., Gao, S., and Schwabacher, M., ''NPARC Simulation and Redesign of the NASA P2 Hypersonic Inlet,'' AIAA Paper 95-2760, July 1995.

[20]Lawrence, C., Zhou, J. L., and Tits, A. L., ''Users Guide for CFSQP Version 2.3: A C Code for Solving (Large Scale) Constrained Nonlinear (Minimax) Optimization Problems, Generating Iterates Satisfying All Inequality Constraints,'' Inst. for Systems Research, Univ. of Maryland, TR-94-16r1, College Park, MD, Nov. 1994.

[21]Gelsey, A., Schwabacher, M., and Smith, D., ''Using Modeling Knowledge to Guide Design Space Search,'' *Artificial Intelligence in Design*, Kluwer, Dordrecht, The Netherlands, 1996, pp. 367–385.

[22]Schwabacher, M. A., ''The Use of Artificial Intelligence to Improve the Numerical Optimization of Complex Engineering Designs,'' Ph.D. Dissertation, Dept. of Computer Science, Rutgers Univ., New Brunswick, NJ, 1996.